RESEARCH ARTICLE

ADVANCED
PHOTONICS
RESEARCH
Open Access

www.adpr-journal.com

Structural Colors Derived from the Combination of Core–Shell Particles with Cellulose

Regina Leiner, Lukas Siegwardt, Catarina Ribeiro, Jonas Dörr, Christian Dietz, Robert W. Stark, and Markus Gallei*

Combining cellulose-based components with functional materials is highly interesting in various research fields due to the improved strength and stiffness of the materials combined with their low weight. Herein, the mechanical properties of opal films are improved by incorporating cellulose fibers and microcrystalline cellulose. This is evidenced by the increase in tensile strength of 162.8% after adding 10 wt% of microcrystalline cellulose. For this purpose, core–shell particles with a rigid, crosslinked polystyrene core and a soft shell of poly(ethyl acrylate) and poly(ethyl acrylate-*co*-hydroxyethyl methacrylate) are synthesized via starved-feed emulsion polymerization. The synthesized particles' well-defined shape, morphology, and thermal properties are analyzed using transmission electron microscopy, scanning electron microscopy, and differential scanning calorimetry measurements. Free-standing mechanochromic opal films with incorporated cellulose and structural colors are obtained after processing the core–shell particles with cellulose via extrusion and the melt-shear organization technique. The homogeneous distribution of the cellulose within the composite material is investigated using fluorescent-labeled cellulose. The opal film's angle-dependent structural color is demonstrated using reflection spectroscopy.

1. Introduction

Cellulose is a renewable and biodegradable biopolymer with excellent availability on Earth due to its abundance in biomass.

R. Leiner, L. Siegwardt, J. Dörr, M. Gallei
Polymer Chemistry
Saarland University
Campus C4 2, Saarbrücken 66123, Germany
E-mail: markus.gallei@uni-saarland.de

C. Ribeiro, C. Dietz, R. W. Stark
Physics of Surfaces, Institute of Materials Science
Technical University of Darmstadt
Peter-Grünberg-Straße 2, Darmstadt 64287, Germany

M. Gallei
Saarene, Saarland Center for Energy Materials and Sustainability
Saarland University
Campus C4 2, Saarbrücken 66123, Germany

Mostly as nanocrystals, cellulose is used in a plethora of research in the field of optical material due to the self-assembly of the helicoidal structures or periodically layered structures leading to a structural color.[1–4] It also features outstanding mechanical, thermal, and wetting properties, depending on the size and the natural resource used to produce the cellulose. Using cellulose to prepare environmentally friendly, functional materials and taking advantage of its intriguing properties is of high interest within the scientific community. Essential features of functional optical materials are the interaction of light with the underlying structures and segments. In the past, researchers were inspired by the optical properties derived from the already-mentioned structural colors found in nature. Famous examples are provided by the morpho butterfly[5] or the opal gemstone.[6] The bright reflection effect of these structural colors occurs due to light interference with periodically arranged microstructures, making dye molecules obsolete. Examples of optical materials that mimic the natural structural color are a broad field of research.[7–9] The most convenient routes to design structurally colored materials based on polymers are drying processes from dispersions of nanoparticles. The hard spheres are arranged on a flat substrate to build colloidal crystals.[10] To avoid crack formations, combinations with sol–gel chemistry are known for synthesizing particle-based polymer films.[11,12] Other examples of opal film formation are the organization techniques focusing on core–shell particles (CSPs).[13,14] The particles feature an elastomeric, and therefore soft shell, which can be pressed through the melt-shear technique at elevated temperatures, allowing the shell to flow, forming a continuous matrix around the core particles. As a rigid core material is used, the core particles do not deform during the processing and arrange due to the shear forces into a colloidal crystal lattice. Due to the periodicity in the arrangement of the particles, a structural color of the processed film is obtained if the core and the surrounding shell material possess different refractive indices.[9,15–17] Following the Bragg–Snell law, the reflected wavelength depends not only on the effective refractive index and the lattice constant of the colloidal crystal but also on the angle of the incident light. This leads to an angle dependency of the reflected color. The mentioned lattice constant is, in the case of a material

made of CSPs, correlated to the particle diameter as it determines the distance between each particle. Under the influence of, for instance, mechanical deformation, this lattice constant changes due to the softening behavior of the shell material and the so-induced displacement of the particles. These changes in the microstructure while maintaining periodicity lead to a mechanochromic color change, rendering the material attractive for smart sensors.[9,18,19]

It is possible to use reinforcement agents as an additive to further improve the aim for the desired thermal and mechanical properties of polymer-based opal materials. For instance, nanocellulose is widely used as an additive in nanocomposites.[20,21] Also, examples of the incorporation of microcrystalline cellulose (MCC) as a reinforcement agent are widely discussed in the literature, for instance, in rubber compounds, with PLA as the matrix or to obtain superabsorbent polymers.[22–24] Besides the effects on the tensile strength, the glass transition temperature, and the rheology,[25,26] the wetting behavior of a compound is also influenced by the addition of the polar cellulose polymer.[27]

Within the present study, the advantage of cellulose and its influence on the mechanical and thermal properties[20] is used in the fabrication of cellulose-incorporated opal films. For this purpose, tailor-made CSPs containing polystyrene (PS) as cores and poly(ethyl acrylate) (PEA) and poly(ethyl acrylate-co-hydroxyethyl methacrylate) (PEA-co-PHEMA) as shell material are synthesized via emulsion polymerization. To obtain a polymer opal film, melt-shear processing is applied, leading to a mechanochromic structural color of the free-standing film as the particles arrange into a colloidal crystal. Cellulose fibers and modified cellulose microcrystals are used as additives during the formation of the opal films to investigate the effect of the cellulose on the tailored CSP-based films. After processing, the obtained opal films are analyzed to determine the influence of the incorporated cellulose on the optical properties, the wetting behavior, and the mechanical stability.

2. Polymer Synthesis and Characterization

In this study, cellulose-incorporated opal films were produced by applying the melt-shear process of core–interlayer–shell particles (CSPs) mixed with cellulose. The CSPs were fabricated via starved-feed emulsion polymerization according to previous works with varying defined sizes to obtain different structural colors due to the difference in the distance between the core particles within the colloidal crystal structure.[9,15,16] Onto the surface of the rigid polystyrene (PS) cores, crosslinked with butanediol diacrylate (BDDA), an interlayer consisting of poly(methyl methacrylate-co-allyl methacrylate) (PMMA-co-PALMA) was polymerized. Two variations of CSPs were synthesized, with the first batch using poly(ethyl acrylate) (PEA) as the outer shell. Those CSPs are labeled PS@PEA. In the second particle synthesis, an outer shell of the copolymer poly(ethyl acrylate-co-hydroxyethyl methacrylate) (PEA-co-PHEMA) was chosen for reasons of possible interactions between the particles and the later added cellulose, resulting in the particles PS@PEA-co-PHEMA. **Scheme 1** shows the preparation route of the crosslinked PS particles and both variations of CSPs.

The core particles, consisting of polystyrene cross-linked with BDDA, were first prepared via starved-feed emulsion polymerization to synthesize the CSPs. The final synthesized particle batch PS-1 featured a hydrodynamic diameter of 185 ± 11 nm, measured via dynamic light scattering (DLS). The size of the particles was also empirically determined via transmission electron microscopy (TEM) measurements, leading to an average size of 164 ± 10 nm (**Figure 1**a).

Two batches of PS particles, PS-1 and PS-2 (cf. Figure S1 in the Supporting Information for further analytical data), were used as core material for polymerizing an interlayer and the outer shell, composed of pure PEA (PS@PEA). Via DLS measurements of the samples, the size evolution of the particles PS-1 after each emulsion polymerization step was visualized, as shown in Figure 1a. Comparing the hydrodynamic diameter of the synthesized CSP PS@PEA-1 of 244 ± 12 nm with the initially used PS-1 cores (185 ± 11 nm), the final CSPs contain an outer shell with a volume fraction of 56 vol%. TEM images show the uniformity of the particles after polymerization of the shell concerning the shape and the dispersity (Figure 1c). The diameter of the CSPs in the dried state is 193 ± 12 nm. Compared with the TEM results of the core particles of 164 ± 10 nm, this corresponds to a volume fraction of 39% shell. The glass transition temperature of the PS
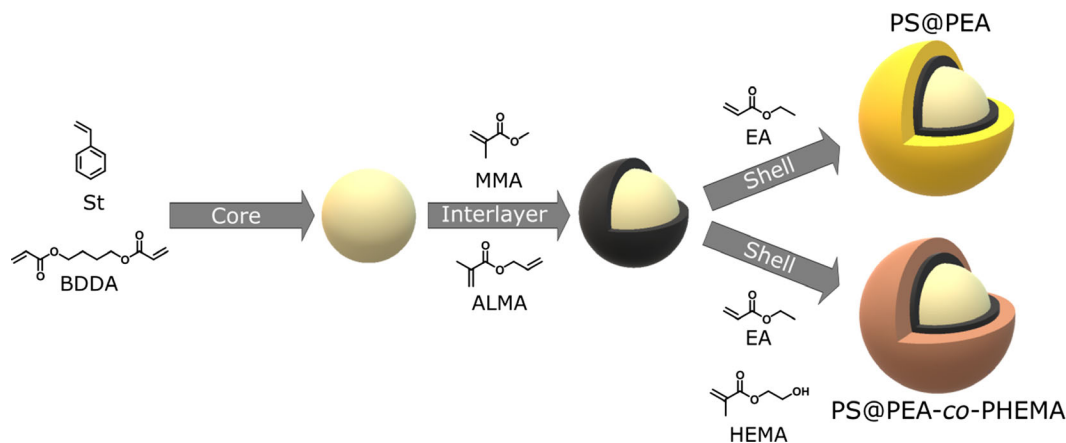
Scheme 1. Synthesis of CSPs using crosslinked polystyrene (with butanediol diacrylate) as core material, PMMA-co-PALMA as interlayer, and PEA (top strategy) or PEA-co-PHEMA (bottom strategy) as the outer shell.
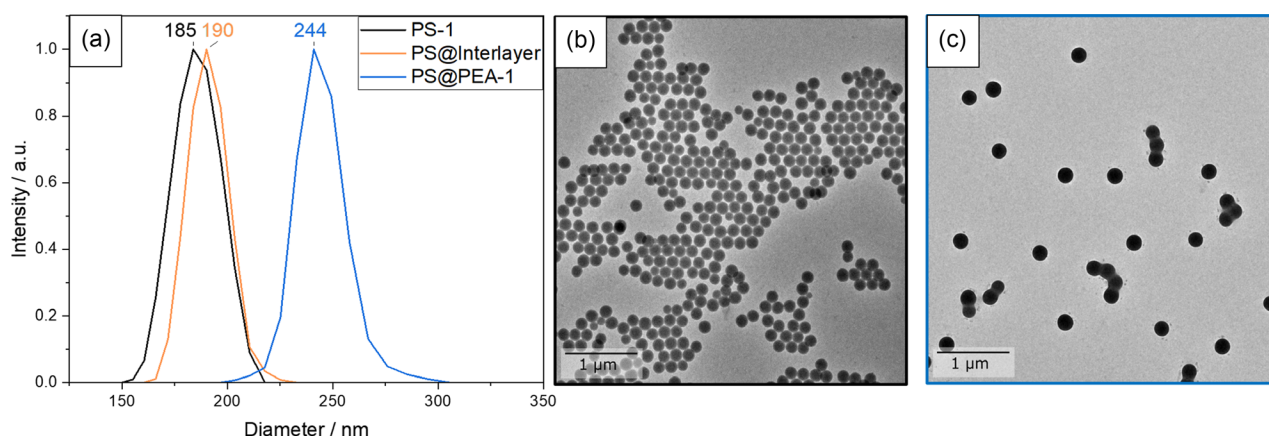
Figure 1. Analyses of the PS@PEA-1 particles. a) DLS measurements of diluted samples after different reaction steps. b) TEM images of the PS-1 cores c) and the PS@PEA-1 CSPs.

Table 1. Overview of the sizes of the synthesized CSPs.

	Core diameter [nm]		CSP diameter [nm]		Core ratio [vol%]	
	DLS	TEM	DLS	TEM	DLS	TEM
PS@PEA-1	185 ± 11	164 ± 10	244 ± 12	193 ± 12	44	61
PS@PEA-2	177 ± 10	106 ± 11	201 ± 10	156 ± 13	68	31
PS@PEA-co-PHEMA-1	205 ± 13	183 ± 18	235 ± 13	233 ± 11	66	48
PS@PEA-co-PHEMA-2	179 ± 13	157 ± 4	283 ± 25	223 ± 38	25	35

core is visible at 114 °C via differential scanning calorimetry (DSC), whereas the shell material shows a T_g of −8 °C (Figure S2). Parallel to this synthesis, a second batch of PS@PEA CSPs was synthesized using PS-2. The sizes of both particle batches were investigated via DLS and TEM (cf. Figure 1 and Figure S1 in the Supporting Information). Their respective calculated amount of the core is given in **Table 1**.

Comparable to the synthesis of the CSPs featuring a shell of pure PEA, other batches of particles were synthesized, using not only ethyl acrylate but also 3 wt% of hydroxyethyl methacrylate (HEMA) as comonomer for the outer shell. The choice of PHEMA as a shell copolymer increased possible interactions with cellulose fibers[28,29] for the intended subsequent introduction into the particle-based film. Equally to the CSPs of PS@PEA, two different batches were synthesized, using PS-3 and PS-4 as core material (Figure S3 and S4 in the Supporting Information). The sizes and compositions of the different synthesized core particles and the corresponding CSPs are compiled in Table 1.

3. Self-Assembly of Cellulose-Based Materials During Opal Film Formation

3.1. Combining the CSPs with Cellulose Fibers in the Dried State

To investigate the self-assembly of the CSPs in the presence of the cellulose fibers in the dried state, two batches of CSPs were used. The PS@PEA-2 emulsion with a solid content of 11% was

mixed with different amounts of the cellulose fiber suspension with a concentration of 6 g L^{-1}, followed by the evaporation of the dispersion medium to obtain composites with a cellulose content of 5 and 50 wt%. The resulting dried mixtures were analyzed via SEM to visualize the distribution of the particles within the cellulose-based materials. The prepared composite materials were compared to the materials derived by the emulsion of CSPs containing a shell with PHEMA (PS@PEA-co-PHEMA-1), as shown in **Figure 2**. An image of the pure cellulose fibers in the absence of particles is shown in Figure S5 in the Supporting Information.

The scanning electron microscopy (SEM) images of the CSPs without cellulose fibers show that the particles self-assembled into hexagonally arranged layers. The CSPs containing PEA and PEA-co-PHEMA as the shell materials showed differences in the surface morphology of the particles under the electron beam. The particles containing only PEA in the outer shell were distinguishable from one another due to the sharper outlines of the monodisperse particles. PHEMA as a copolymer in the shell led to more indistinct outlines as the CSPs softened faster under the electron beam than the PEA particles. As 5 wt% cellulose fibers were added to the particles, the CSPs were arranged on the surface of the cellulose fibers rather than drying separately from the fibers. It is possible that the particles could adhere to the fiber surface due to the coarse surface structure of the fibers. Increasing the number of cellulose fibers to 50 wt%, the hexagonal assembly of the particles onto the cellulose fibers was still present even at this high cellulose fiber content. To further demonstrate the arrangement of the PEA-co-PHEMA particles at the cellulose fibers, the fibers were immersed into the
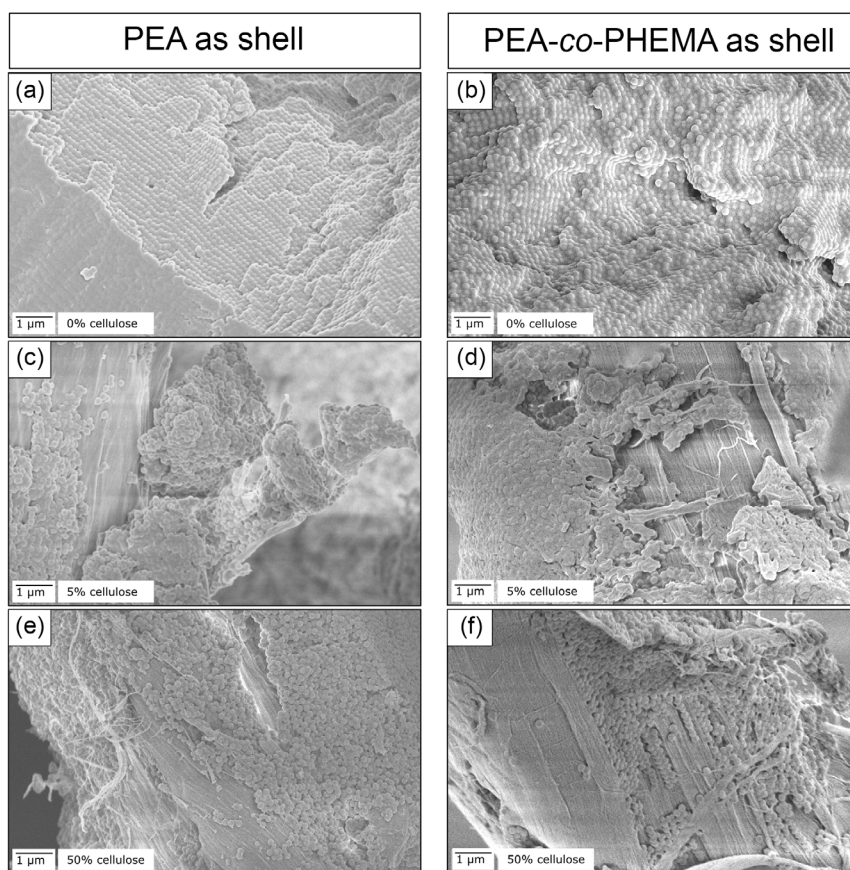
Figure 2. SEM images of the CSPs with PEA (left) and PEA-*co*-PHEMA (right) as shell material mixed with varying content of cellulose fibers (a,b: 0 wt%. c,d: 5 wt%. e,f: 50 wt%).
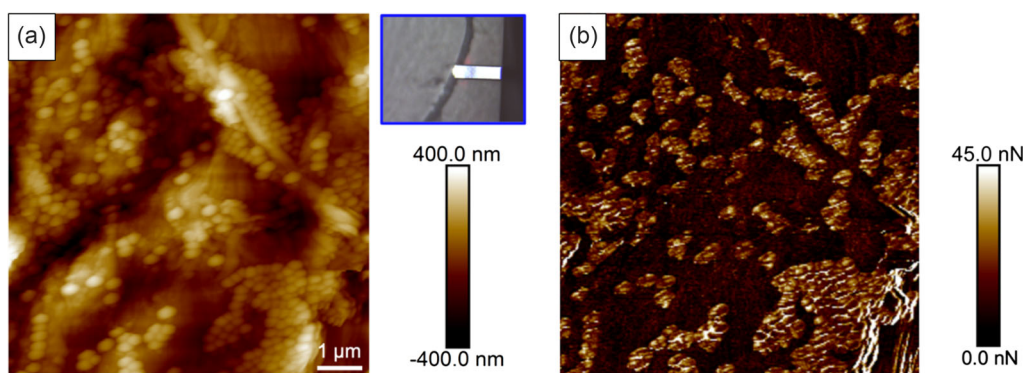

Figure 3. a) AFM topography image of PEA-*co*-PHEMA particles adsorbed on a single cotton linter cellulose fiber. b) Corresponding adhesion image in which particles stand out from the fiber. The inset (blue framed optical image) shows the measurement position where the AFM image was taken.

particle solution by drop casting (see Experimental Section). **Figure 3** shows an atomic force microscopy (AFM) image taken in the middle of the fiber after drying the dispersion of the PEA-*co*-PHEMA shell particles. The topographic image (Figure 3a) exhibited a homogeneous distribution of particles within the arbitrarily selected area comprising agglomerates at the amorphous regions of the cellulose fiber. The corresponding adhesion image (Figure 3b) clearly showed distinct adhesion values for the

PEA-*co*-PHEMA particles compared to the adhesion values for the cellulose fiber. The dense distribution of the adhered particles showed their affinity to the fibers, similar to the results in Figure 2. However, a distinct influence of the hydroxy moieties close to the cellulose fiber surface cannot be accentuated here, as surface roughness and residual polar moieties from the initiator stemming from the emulsion polymerization might also play a crucial role. In the following and for the investigation of the

optical properties, the PEA- and PEA-*co*-PHEMA-containing core-shell particles are not distinguished, as neither the order at the fibers' surfaces nor the refractive index of the different polymethacrylates were different.

In conclusion to the SEM and AFM studies, the adhesion and hexagonal arrangement of the CSPs onto the fibers featured a specific interaction of the particle shell to the fibers' surface. Even at a high content of cellulose fibers of 50 wt%, the assembly of the particles was observed.

3.2. Opal Film Formation in the Presence of Microcrystalline Cellulose

To investigate the combination of MCC with polymer opal materials similarly, the CSPs were extruded, and the extruder strands were further processed applying the melt-shear organization method. A simplified scheme of this process is shown in Figure S6. MCC was added during extrusion to incorporate cellulose into these films to guarantee a homogeneous distribution within the material. To visualize the cellulose microcrystals and their distribution inside the material, they were covalently modified with the fluorescent label fluorescein by following the synthetic route shown in **Figure 4**a. Inspired by the previously reported functionalization of porous polymer microparticles containing primary hydroxyl groups,[30] an adapted protocol was applied to introduce fluorescein as its isothiocyanate derivative by addition reaction to the free hydroxyl groups of the cellulose. The reaction occurred in dimethylacetamide (DMAc) as the appropriate suspension agent for the cellulose and pyridine as the basic suspension medium (see Experimental Section).

After 20 h of stirring at ambient temperature, the yellow-colored product was precipitated and washed with EtOH until the fluorescence of the washing solvent under UV light disappeared. The dried product was analyzed via attenuated total reflection Fourier-transform infrared (ATR–FTIR) spectroscopy. The corresponding spectrum, shown in Figure 4b, gives the typical signals for cellulose, containing the OH stretching mode at 3100–3550 cm^{-1}, the C–H stretching at 2899 cm^{-1}, and the O–H signal of absorbed water at 1642 cm^{-1}. The signal at 1430 cm^{-1} corresponds to the CH$_2$ symmetric bending, and at 1373 cm^{-1}, the C–H bending is visible. The C–O–C stretching mode of the ring corresponds to the signal at 1032 cm^{-1}, the signal at 898 cm^{-1} belongs to the C–O–C β-glycosidic linkage, and at 664 cm^{-1}, the O–H vibrations are visible. The absence of an isothiocyanate vibration led to the assumption of successful functionalization and complete removal of the residual isothiocyanate.

Through the functionalization of the MCC with fluorescein, the homogeneous distribution of the cellulose within the CSP films could be proven via analysis of the reflected color of the processed films. After adding 5 wt% of the fluorescein-functionalized MCC, the processed film homogeneously featured a yellow color all over the film stemming from the fluorescent dye, as can be concluded from the photograph in **Figure 5**. Permitting transmission effects through the film, for example, with the help of a white background, the cellulose-CSP film showed a yellow color compared to the white film, where no cellulose was incorporated (Figure 5a). Supressing transmission through a black surface, the blue structural color at a wavelength of 488 nm from the periodically arranged CSPs in the pure opal film was apparent in both opal films (Figure 5b,c). While applying
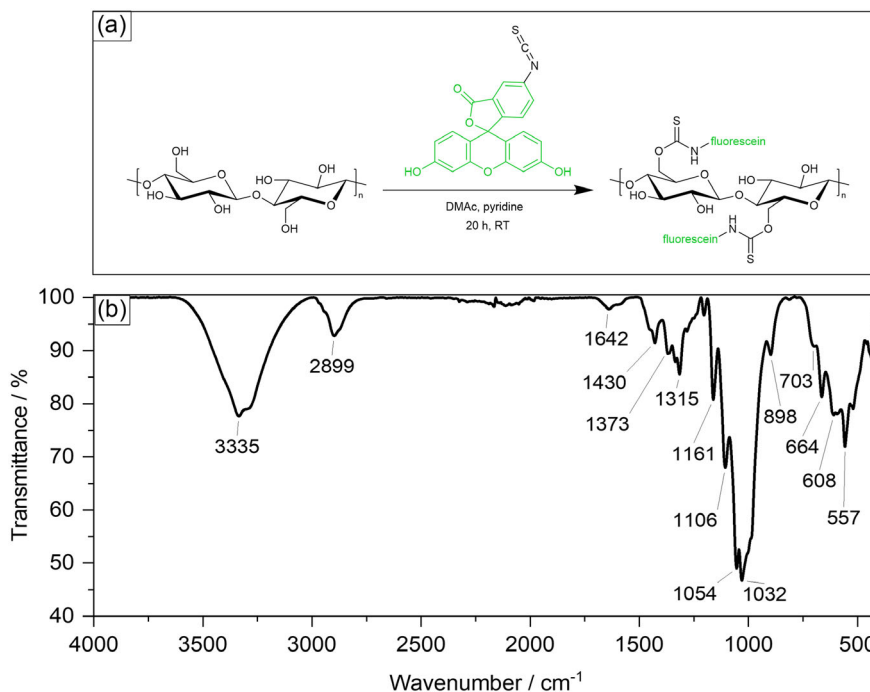

Figure 4. a) Reaction scheme of the functionalization of MCC with fluorescein (marked green) using fluorescein isothiocyanate and b) corresponding ATR–FTIR spectrum of the product.
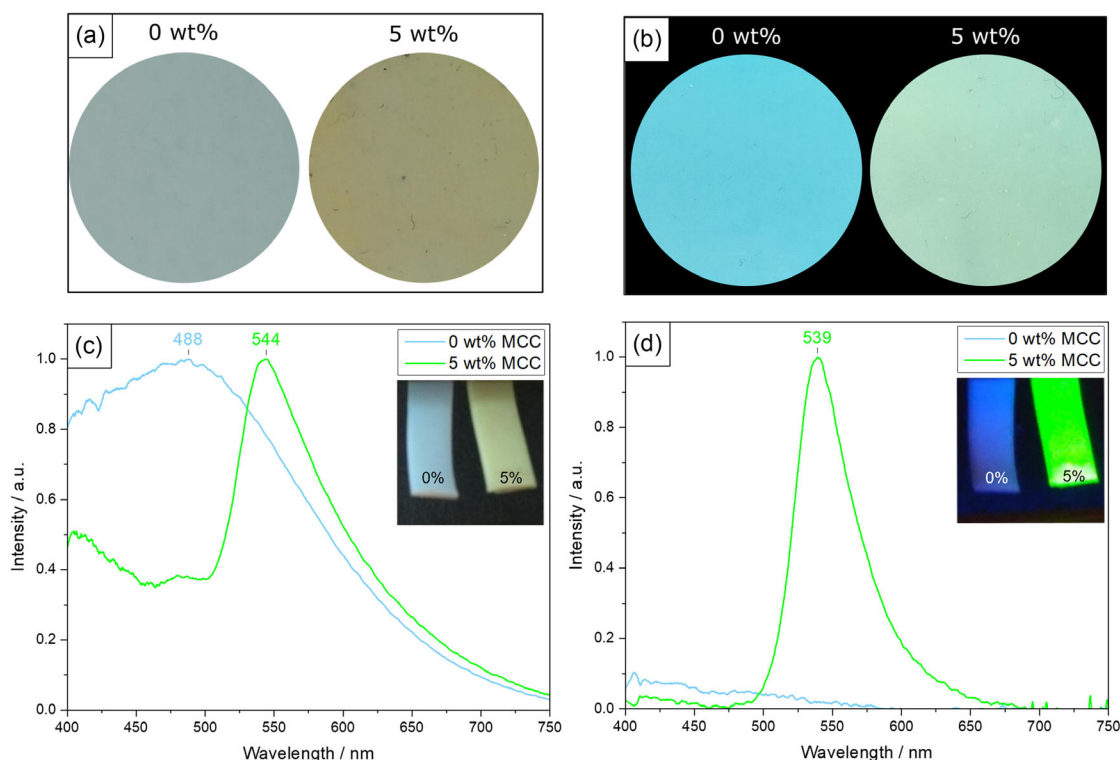
**ADVANCED
SCIENCE NEWS**

www.advancedsciencenews.com

**ADVANCED
PHOTONICS
RESEARCH**

www.adpr-journal.com

Figure 5. Opal films of PS@PEA-*co*-PHEMA-2 with incorporated fluorescent MCC using a) a white and b) a black background for different optical effects. c) Normalized reflection spectra under visible light and d) under UV light at 366 nm.

UV irradiation, the functionalized MCC's bright fluorescence at 539 nm was visible (Figure 5d). As the core particles consisted of polystyrene, a weak fluorescent response of the pure polymer material in the blue region was also present. In conclusion, incorporating MCC into the polymer opal films through extrusion led to a homogenous distribution of cellulose within the matrix.

The CSPs containing PEA as the outer shell polymer were mixed with 5.0, 7.5, and 10 wt% of functionalized MCC during extrusion. An amount of 0.03 wt% of carbon black, known to improve the opal structural color of the film, was also added during extrusion.[31,32] Photographs of the opal films after the applied melt-shear process are depicted in **Figure 6**a. Contact angle measurements of the processed films displayed decreased contact angle at increasing cellulose content (Figure S7). The increase in hydrophilicity indicated the successful incorporation of the MCC and the influence of the cellulose microcrystals on the wetting behavior of the composite. Comparing the optical properties of the composites with different contents of MCC to the pure polymer film, the structural colors were similar, even after adding 10 wt% of the yellow, fluorescein-modified cellulose. This led to the conclusion that the cellulose was well distributed inside the opal films so that the colloidal crystal structure of the CSPs was not negatively affected. The structural color of the films was further analyzed by measuring the reflection spectra at visible light to prove the angle dependency of the reflective colors. Varying the position of the light source led to the expected blueshift in the emission of these samples, as shown in Figure 6b,c and the Supporting Information (Figure S8). Analyzing the

signals at an angle of the incident light of 50° onto the films containing the fluorescent-labeled MCC, a second peak at 530 nm became visible, corresponding to the emission maxima of the dye.[33] From these results, it was concluded that the yellow color induced by the addition of the MCC did not interfere with the structural color of the polymer opal film, as carbon black was used.

The structural color also changed after applying mechanical stress to the films. By applying stress, the soft polymer representing the shell material flowed around the rigid cores, rearranging the particles. Due to the Bragg–Snell law, the new distance between the cores led to the structural color change.[9,34] This mechanochromic behavior of the cellulose-incorporated composites was visible during tensile strength measurements. As shown in **Figure 7**a, the color of the pure polymer film shifted from a turquoise color to dark blue at increasing elongation ε. The sample with 10 wt% incorporated cellulose showed the same blueshift (Figure 7b). The tensile strength measurements exhibited a higher tensile strength of the material with an increasing content of the MCC (Figure 7c). It can, therefore, be concluded that the addition of MCC led to a reinforcement of the composite material. Besides the evaluation of the tensile strength, the elongation behavior of the composites was investigated. As shown in Figure 7c, the elongation of the samples until breakage decreased with an increasing MCC content.

In conclusion, the homogeneous distribution of the MCC influenced the mechanical properties in terms of a higher tensile strength and a decreasing stretching capability.
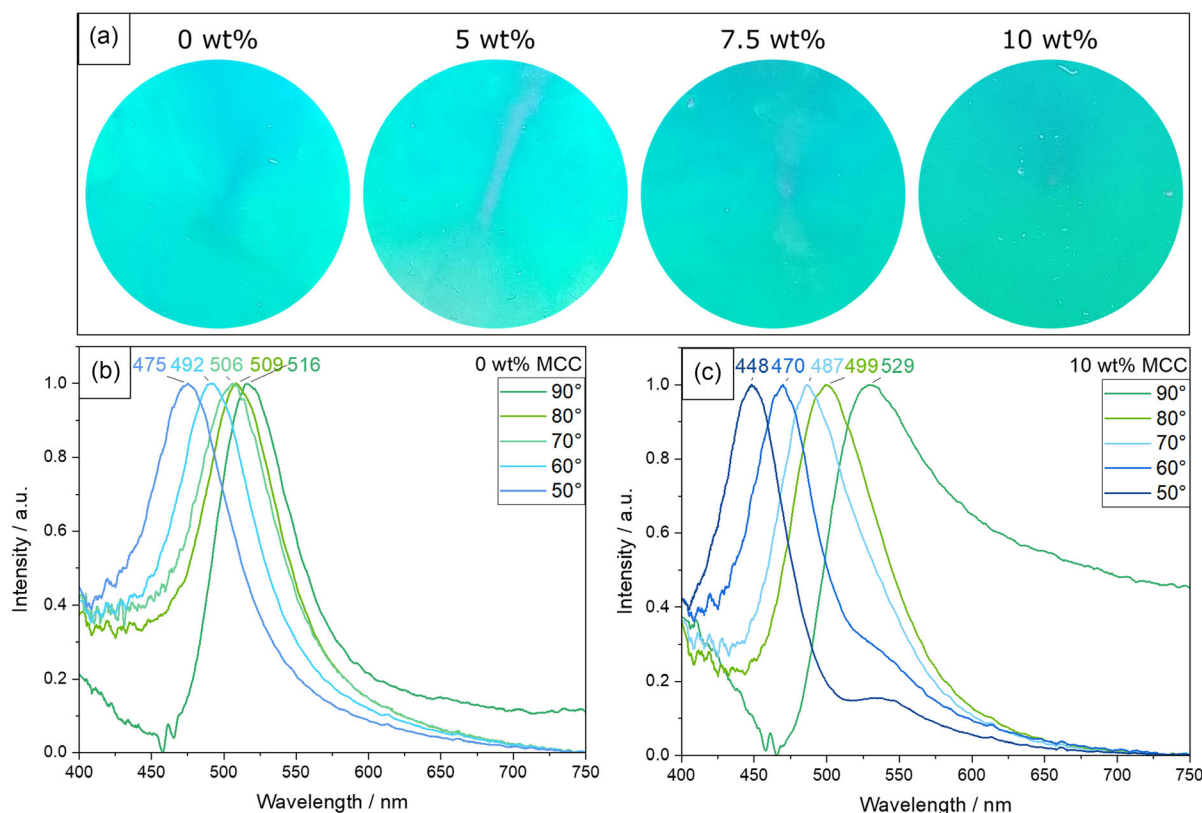
Figure 6. a) Photographs and b,c) normalized angle-dependent reflection spectra of the opal films prepared from PS@PEA-1 CSPs with different amounts of MCC.
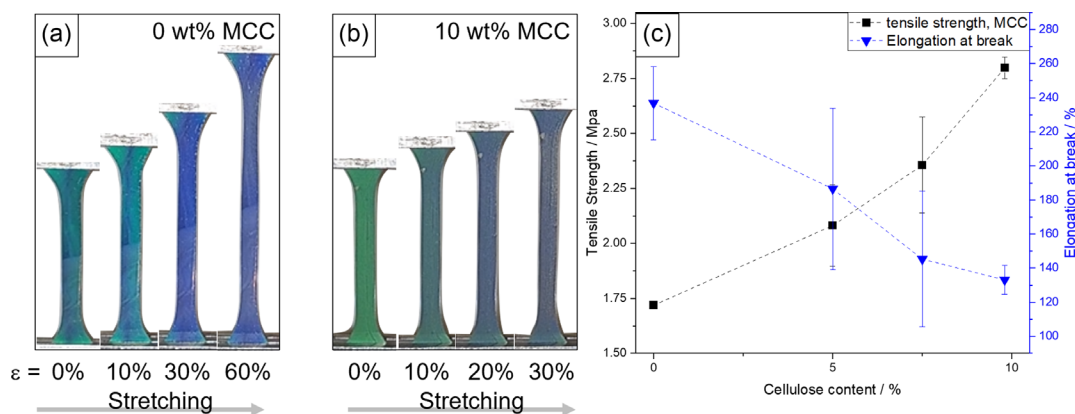

Figure 7. Tensile strength tests of the composites of PS@PEA-1 with incorporated MCC. a) Color change during elongation of the samples with 0 wt% MCC and b) with 10 wt% MCC. c) Influence of the content of MCC on the tensile strength and the elongation at break.

4. Conclusion

Core–shell nanoparticles with PS as the core material and either PEA or PEA-*co*-PHEMA as the outer shell materials were synthesized using starved-feed emulsion polymerization. Via SEM imaging and AFM measurements, the arrangement of the particles in the presence of cellulose fibers in a dry state was displayed, concluding that the particles self-assembled and were well-ordered onto the fibers. The CSPs were processed by applying the melt-shear organization technique to produce freestanding opal films. Fluorescent-labeled MCC was successfully prepared and incorporated into the opal materials via extrusion. From investigations of these hybrid cellulose–opal films, a homogeneous distribution of the MCC could be proven. Moreover, by incorporating MCC, the mechanical properties were enhanced, as depicted by the increased tensile strength of 162.8% as

**ADVANCED
SCIENCE NEWS**

www.advancedsciencenews.com

**ADVANCED
PHOTONICS
RESEARCH**
Open Access

www.adpr-journal.com

10 wt% of the MCC was incorporated. During the tensile strength tests, the mechanochromic behavior of the composites was displayed. Even the composites with a high cellulose content of 10 wt% exhibited an angle-dependent structural color. Consequently, the nanoparticles maintained the periodic arrangement as a colloidal crystal without being restricted by incorporating the larger cellulose microcrystals, which would lead to a loss of structural color. The results show that cellulose acts as a reinforcement agent while maintaining the structural color and mechanochromic behavior of polymer opal films. Combining cellulose with opaline structurally colored materials will pave the way for new anticounterfeiting materials with improved stability and wettability in different fields of optical sensors.

5. Experimental Section

Characterization: DLS was measured using a Zetasizer Nano ZS90 (Malvern, UK) equipped with a 4 mW, 633 nm HeNe laser at 25 °C. Size determination was performed at an angle of 90° with a fivefold determination of 15 runs using polystyrene cuvettes. Automated data acquisition in 300 size classes and peak determination was done using Zetasizer Nano software. The intensities were normalized to the highest signal in each measurement. For TEM imaging, the diluted polymer dispersions were drop cast on a carbon-coated copper grid. The dispersion medium evaporated at ambient conditions for at least 12 h. The TEM experiments were carried out using a JEOL JEM-2100 LaB6 electron microscope (JEOL Ltd. Tokyo, Japan) at a nominal acceleration voltage of 200 kV with a Gatan Orius SC100 CCD camera in bright-field mode. The particle sizes were analyzed using the software ImageJ. For SEM, the particle samples were mounted on an Al stud using carbon tape and coated with 6 nm platinum using an Automatic Turbo Coater PLASMATOOL 125 SIN 2020_131 from Ingenieurbüro Peter Liebscher. The measurements were carried out on a Zeiss Gemini500 Sigma VP device using the software SmartSEM Version 6.07, with accelerating voltages between 2 and 4 kV. DSC was carried out with a Netzsch 214 Polyma with a heating rate of 10 K min^{-1} and a sample mass of 5.0 mg. Each glass transition temperature was determined using Netzsch Proteus software. Tensile tests were performed using a Zwick/ Roell universal testing machine with a testing speed of 1.0 mm s^{-1}. Data was obtained using testXpert II. Reflection spectra were recorded using an Ocean Optics fiber FLAME vis/NIR fiber spectrometer USB2000, combined with an Ocean Optics deuterium/tungsten halogen lamp DT mini 2. All spectra were recorded in reflection mode. Peak wavelengths were determined using OceanView software. Reflection intensities were normalized to the highest value in each measurement series after smoothing the curves every 40 points for better visualization. For angle-dependent measurements, the spectrometer was operated in θ–2θ mode. An angle of $\theta = 90°$ refers to normal incidence. FTIR spectra were acquired on an ATR–FTIR (diamond ATR) instrument (Bruker Alpha II) in the 400–4000 cm^{-1} range with a resolution of 4 cm^{-1}. Contact angle measurements were performed using a Hamilton syringe 100 µL in a syringe pump by kdScientific adjusted to 10 µL and a custom xyz positioning table. Photographs were collected using a Nikon D54000 and digiCamControl 2.1.2.0, open drop 3.3.1 was used for evaluation. For AFM, a single cotton linter fiber was pulled out of a paper mesh with a pair of tweezers and fixed on a glass substrate with nail polish at its ends. The stock solution containing the PEA-*co*-PHEMA particles was diluted 1:100 with deionized water. Subsequently, 10 µL of the diluted solution was drop cast onto the prepared fiber. Once the solution dried at room temperature, AFM analysis was performed using a Dimension Icon atomic force microscope (Bruker AXS, Santa Barbara, CA) in the PeakForce tapping mode. An NSC35 cantilever (µMasch, Sofia, Bulgaria) with a force constant of $k = 16.1$ N m^{-1} calibrated by the thermal noise method[35] was used. Images were taken at a tip velocity of 8 µm s^{-1} at a constant peak force of 40 nN and an excitation frequency of 2 kHz (100 nm oscillation amplitude).

Reagents: Styrene (St, 99%) and hydroxyethyl methacrylate (HEMA, 97%) were purchased from Fisher Scientific. Butanedioldiacrylate (BDDA, 90%), methylmethacrylate (MMA, 99%), and ethylacrylate (EA, 99.5%) were purchased from Sigma-Aldrich. Allyl methacrylate (ALMA, 98%) was purchased from TCI. Before emulsion polymerization, stabilizing agents were removed from the monomers by passing them through a basic alumina column (50–200 µm, Acros Organics). Potassium hydroxide flakes (KOH, 90% reagent grade), sodium disulfite (NaDS, analysis grade), sodium persulfate (NaPS, ≥98%), and sodium dodecyl sulfate (SDS, ≥98.5%) were purchased from Sigma-Aldrich. Dowfax2A1 was purchased from EZkem. Carbon black (Channel Type Black 4) was obtained from Evonik. Cellulose linters fibers were used in aqueous suspension with a concentration of 6 g L^{-1}. As MCC, Avicel PH-101 from Fluka was used. 4-Fluorophenyl isocyanate (99%) was purchased from Sigma Aldrich.

Exemplary Synthesis of Crosslinked Polystyrene Particles: Crosslinked polystyrene core particles were synthesized in a 250 mL double-walled reactor equipped with a reflux condenser and a stirrer under a nitrogen atmosphere at 75 °C. The vessel was filled with a monomer emulsion of 1.53 g St, 0.17 g BDDA, 0.09 g SDS, and 120 g deionized water. While stirring at 300 rpm, the polymerization was subsequently initiated with 0.03 g NaDS and 0.22 g NaPS. After a reaction time of 8 min, a monomer emulsion (ME0) containing 28.20 g St, 2.82 g BDDA, 0.09 g SDS, 0.16 g KOH, 0.09 g Dowfax2A1, and 36 g deionized water was added continuously with a flow rate of 1.0 mL min^{-1}, using a rotary piston pump (Ismatec reglo-CPF digital, RH00). After adding the ME0, the reaction was stirred for 30 min. Further batches of crosslinked PS particles were synthesized with minor adjustments. More detailed information about these syntheses can be found in the Supporting Information.

Exemplary Polymerization of the Interlayer and the Outer Shell: For the starved-feed emulsion polymerization of the core-interlayer-shell particles containing only PEA in the outer shell, the above-described crosslinked PS particles were used as core material. The particle emulsion was diluted to a solid content of 8.00 wt%. 294 g of the diluted core particle emulsion was filled in a 1 L double-walled reactor equipped with a reflux condenser and a stirrer under nitrogen atmosphere at 85 °C. While stirring at 200 rpm, the emulsion polymerization was initiated by adding 0.09 g NaDS and 0.52 g NaPS. After a reaction time of 15 min, a monomer emulsion (ME1) containing 5.05 g MMA, 0.56 g ALMA, 0.10 g Dowfax2A1, 0.05 g SDS, and 22.66 g deionized water was continuously added with a constant flow rate of 1.5 mL min^{-1} using a rotary piston pump. After adding ME1 and an additional 15 min, the emulsion polymerization was reinitiated by adding 0.08 g NaPS and continuously stirred for another 10 min. Afterward, a second monomer emulsion (ME2) containing 0.26 g SDS, 0.21 g Dowfax2A1, 0.36 g KOH, and 85.12 g deionized water was prepared. For synthesizing CSPs with PEA in the outer shell, 65.19 g EA was added as monomers to the ME2. While preparing the CSPs with PEA-*co*-PHEMA as the shell, a mixture of 3 wt% HEMA and 97 wt% EA was used as monomer in ME2. The monomer emulsion was continuously added to the reinitiated particles with a flow rate of 1.5 mL min^{-1} using a rotary piston pump. After adding ME2, the reaction mixture was kept at a constant temperature and stirred for an additional hour. Further batches of equivalent core-interlayer-shell particles were synthesized following the described route with minor adjustments. More detailed information can be found in Table S1 in the Supporting Information.

Functionalization of Microcrystalline Cellulose (MCC): The functionalization of MCC with fluorescein isothiocyanate occurred inspired by an already published method.[30] Here, predried MCC (1.00 g, 1.0 eq.) was suspended in DMAc (20 mL) and pyridine (5 mL). Fluorescein isothiocyanate (5.0 mg, 0.01 eq. per AGU) was added, and the reaction mixture was stirred for 20 h at room temperature and precipitated by dropwise in addition to vigorously stirred EtOH (150 mL). The resulting suspension was filtrated, and the residue was washed with EtOH until no more fluorescent emission was visible in the washing solvent under UV light. After drying at 40 °C under reduced pressure for 24 h, the product was obtained as a light-yellow solid.

ADVANCED
SCIENCE NEWS

www.advancedsciencenews.com

ADVANCED
PHOTONICS
RESEARCH
Open Access

www.adpr-journal.com

Processing: Compounds with cellulose fibers were fabricated by mixing the CSP emulsion with the cellulose suspension and evaporating the water at ambient temperature. To obtain opal material with structural color, the CSPs were freeze dried and mixed with 0.03 wt% carbon black (Evonik Channel Type Black 4, particle size <45 μm) before being extruded at 90 °C and 25 rpm (Thermo Scientific HAAKE MiniLab 3 Micro-Compounder). The incorporation of MCC occurred during the extrusion of the freeze-dried particles. For opal film formation, the extruded samples were covered between two polyethylene terephthalate (PET) foils and inserted into a Collin laboratory press P200 P/M (Dr. Collin GmbH, Ebersberg, Germany) and pressed at 95 °C and with a pressure of 10 bar for 3 min.

Supporting Information

Supporting Information is available from the Wiley Online Library or from the author.

Conflict of Interest

The authors declare no conflict of interest.

Author Contributions

Regina Leiner: Conceptualization (lead); Data curation (lead); Formal analysis (lead); Investigation (lead); Methodology (lead); Validation (lead); Visualization (lead); Writing—original draft (lead); Writing—review and editing (lead). Lukas Siegwardt: Data curation (equal); Formal analysis (equal); Investigation (equal); Methodology (equal); Validation (equal). Catarina Ribeiro: Data curation (supporting); Formal analysis (supporting); Methodology (equal); Validation (supporting). Jonas Dörr: Data curation (supporting); Formal analysis (equal); Investigation (supporting); Methodology (supporting); Validation (equal); Writing—review and editing (supporting). Christian Dietz: Data curation (equal); Formal analysis (equal); Investigation (equal); Methodology (equal); Validation (equal); Visualization (supporting); Writing—review and editing (supporting). Robert W. Stark: Funding acquisition (equal); Methodology (supporting); Project administration (supporting); Resources (supporting); Software (supporting); Supervision (supporting); Writing—review and editing (supporting). Markus Gallei: Conceptualization (lead); Data curation (equal); Funding acquisition (lead); Investigation (equal); Project administration (lead); Resources (lead); Software (lead); Supervision (lead); Validation (lead); Visualization (equal); Writing—original draft (lead); Writing—review and editing (lead).

Data Availability Statement

Research data are not shared.

Keywords

bio-based composites, cellulose, core–shell particles, emulsion polymerizations, nanocomposites, nanoparticles structural colors

[1] A. R. Quelhas, A. C. Trindade, *Crystals* **2023**, *13*, 1010.
[2] R. M. Parker, T. G. Parton, C. L. C. Chan, M. M. Bay, B. Frka-Petesic, S. Vignolini, *Acc. Mater. Res.* **2023**, *4*, 522.
[3] B. Frka-Petesic, T. G. Parton, C. Honorato-Rios, A. Narkevicius, K. Ballu, Q. Shen, Z. Lu, Y. Ogawa, J. S. Haataja, B. E. Droguet, R. M. Parker, S. Vignolini, *Chem. Rev.* **2023**, *123*, 12595.
[4] R. M. Parker, T. H. Zhao, B. Frka-Petesic, S. Vignolini, *Nat. Commun.* **2022**, *13*, 3378.
[5] S. Yoshioka, S. Kinoshita, *Proc. R. Soc. B Biol. Sci.* **2006**, *273*, 129.
[6] J. V. Sanders, *Nature* **1964**, *204*, 1151.
[7] C. G. Schafer, C. Lederle, K. Zentel, B. Stuhn, M. Gallei, *Macromol. Rapid Commun.* **2014**, *35*, 1852.
[8] D. Scheid, C. Lederle, S. Vowinkel, C. G. Schäfer, B. Stühn, M. Gallei, *J. Mater. Chem. C* **2014**, *2*, 2583.
[9] C. G. Schafer, B. Viel, G. P. Hellmann, M. Rehahn, M. Gallei, *ACS Appl. Mater. Interfaces* **2013**, *5*, 10623.
[10] P. Jiang, J. F. Bertone, K. S. Hwang, V. L. Colvin, *Chem. Mater.* **1999**, *11*, 2132.
[11] B. Hatton, L. Mishchenko, S. Davis, K. H. Sandhage, J. Aizenberg, *Proc. Natl. Acad. Sci. U.S.A.* **2010**, *107*, 10354.
[12] Y. Vasquez, M. Kolle, L. Mishchenko, B. D. Hatton, J. Aizenberg, *ACS Photonics* **2014**, *1*, 53.
[13] M. Gallei, *Macromol. Rapid Commun.* **2018**, *39*, 1700648.
[14] Q. Zhao, C. E. Finlayson, D. R. Snoswell, A. Haines, C. Schäfer, P. Spahn, G. P. Hellmann, A. V. Petukhov, L. Herrmann, P. Burdet, P. A. Midgley, S. Butler, M. Mackley, Q. Guo, J. J. Baumberg, *Nat. Commun.* **2016**, *7*, 11661.
[15] L. Siegwardt, M. Gallei, *Chem. Eng. J.* **2024**, *480*, 148168.
[16] L. Siegwardt, M. Gallei, *Adv. Funct. Mater.* **2023**, *33*, 2213099.
[17] M. Bitsch, A. K. Boehm, A. Grandjean, G. Jung, M. Gallei, *Molecules* **2021**, *26*, 7350.
[18] C. G. Schäfer, G. P. Hellmann, M. Rehahn, M. Gallei, *J. Nanophotonics* **2013**, *7*, 070599.
[19] C. G. Schäfer, M. Gallei, J. T. Zahn, J. Engelhardt, G. P. Hellmann, M. Rehahn, *Chem. Mater.* **2013**, *25*, 2309.
[20] F. Fahma, I. Febiyanti, N. Lisdayana, I. W. Arnata, D. Sartika, *Arch. Mater. Sci. Eng.* **2021**, *2*, 49.
[21] A. Dufresne, *Mater. Today* **2013**, *16*, 220.
[22] S. K. Bhattacharyya, B. S. Parmar, A. Chakraborty, S. Dasgupta, R. Mukhopadhyay, A. Bandyopadhyay, *Ind. Eng. Chem. Res.* **2012**, *51*, 10649.
[23] A. P. Mathew, K. Oksman, M. Sain, *J. Appl. Polym. Sci.* **2005**, *97*, 2014.
[24] T. Dumkor, S. Poompradub, *Int. J. Biol. Macromol.* **2023**, *233*, 123556.
[25] S. Mohan Bhasney, A. Kumar, V. Katiyar, *Comp. Part B: Eng.* **2020**, *184*, 107717.
[26] D. Krapez Tomec, M. Schoflinger, J. Lesslhumer, U. Gradisar Centa, J. Zigon, M. Kariz, *Polymers* **2024**, *16*, 836.
[27] M. C. Popescu, B. I. Dogaru, C. M. Popescu, *Mater. Design* **2017**, *132*, 170.
[28] M. Plank, F. Hartmann, B. Kuttich, T. Kraus, M. Gallei, *Eur. Polym. J.* **2020**, *141*, 110059.

[29] L. Gemmer, Q. Hu, B.-J. Niebuur, T. Kraus, B. N. Balzer, M. Gallei, *Polym. Chem.* **2022**, *13*, 4028.

[30] D. Schmitt, S. M. Abdel-Hafez, M. Tummeley, V. Schünemann, M. Schneider, V. Presser, M. Gallei, *Macromolecules* **2023**, *56*, 7086.

[31] O. L. Pursiainen, J. J. Baumberg, H. Winkler, B. Viel, P. Spahn, T. Ruhl, *Opt. Express* **2007**, *15*, 9553.

[32] L. Siegwardt, V. Glößner, A. Boehm, M. Schneider, M. Gallei, *ACS Appl. Mater. Interface* **2024**, *16*, 10722.

[33] M. M. Martin, L. Lindqvist, *J. Lumin.* **1975**, *10*, 381.

[34] T. Ding, G. Cao, C. G. Schäfer, Q. Zhao, M. Gallei, S. K. Smoukov, J. J. Baumberg, *ACS Appl. Mater. Interface* **2015**, *7*, 13497.

[35] H. J. Butt, M. Jaschke, *Nanotechnology* **1995**, *6*, 1.